Random-walk simulation of non-conservative pollutant transport in shallow water flows

Fan Yang[1], Dongfang Liang[1,*]

[1]Department of Engineering, University of Cambridge, Trumpington Street, Cambridge CB2 1PZ, United Kingdom

[*]Corresponding author: Dr. Dongfang Liang, dl359@cam.ac.uk

Abstract

The random-walk method is inherently simple and numerically stable. However, when used in hydro-environmental analyses, most of the existing random-walk methods ignore the influence of the non-uniform water depth and only consider the transport of inert materials, hence the inability of modelling biochemical reactions. In addition, they mainly examine the instantaneous-release problems, with a fixed number of particles moving in the computational domain. This paper first presents examples to showcase the capability of the newly developed model in simulating the continuous source of non-conservative substances. Then, the method is applied to simulate the BOD-DO balance along a hypothetical river. The numerical results agree well with the analytical solutions. Finally, the developed model is used to study the pollutant transport in the Thames Estuary. The current model is illustrated to be able to accurately predict the interaction between multiple pollutants in real-world situations with uneven bathymetry and extensive intertidal floodplains.

Key words: random walk method; solute transport; water pollution; advection; diffusion; water quality modelling

1. Introduction

Water quality deterioration has detrimental impacts on the environment, which may threat human health and result in significant economic losses. Accurate and efficient water quality estimation is essential for establishing a control strategy for environmental protection (Benkhaldoun et al. 2007). In the past few decades, increasing emphasis has been placed on the numerical modelling of water quality status in estuarine, coastal and river waters (Lin and Roger 1997; Gupta et al. 2004; Murillo et al. 2006). These water bodies have some common characteristics, such as shallow water depth, high biochemical activity, uneven bathymetry and complex geometry (Yuan 2007). In these shallow waters, the horizontal scale is usually

much larger than the vertical scale, so the solute is often assumed to be well-mixed vertically over the water column. Many horizontal two-dimensional (2-D) models have been successfully developed to predict the flow fields and solute transport processes in these shallow-water environments (Murillo et al. 2005; Burguete et al. 2006; Pu 2016). Most of them rely on the mesh-based methods to solve the standard shallow water equations and advection-diffusion equations using finite-difference or finite-element techniques (Lin and Falconer, 1997; Mingham et al. 2001; Benkhaldoun and Mohammed, 2007). However, these Eulerian approaches tend to produce artificial diffusion when addressing steep concentration gradients and are sensitive to the mesh resolution (Liang et al. 2006; Yang et al. 2018). Thanks to advanced computing techniques, increasing level of attention has been paid to Lagrangian approaches in computational hydraulics, which have higher levels of stability and simplicity than mesh-based methods (Pu et al. 2016; Kazemi et al. 2017; Zheng et al. 2017).

The random walk method is a typical mesh-free approach for modelling pollutant transport (e.g. Israelsson et al. 2005; Liang and Wu 2014). It originates from statistical physics and has been applied in many disciplines such as finance, biology and hydrology. In modelling solute transport, the random walk method tracks the movement of discrete particles, which serve as indicators to represent the pollutant cloud. Israelsson et al. (2005) summarised the strengths and weaknesses of three Lagrangian techniques and concluded that the random walk method is most accurate and flexible. Wu and Liang (2019) and Yang et al. (2020) proved that the random walk method can achieve higher accuracy than Eulerian models and is better suited to the situation with high contamination gradients. This method is attractive for several reasons: (1) perfectly conservative by definition, (2) capable of resolving steep concentration gradients with high accuracy, (3) efficient when pollutant clouds only occupy a small area of the computational domain.

Because a large number of particles are needed to obtain smooth concentration distributions, the random walk method is often thought to require more computational resources than the mesh-based method. The computational cost of the traditional mesh-based model depends on the mesh resolution and the time step, with the latter often limited by the Courant–Friedrichs–Lewy condition. The computational cost of the random walk model depends the number of particles and the time step. Wu et al. (2019) showed that large time steps can be used without sacrificing accuracy or stability. The relative computational efficiency of the different models depends on the studied problems. The mesh-based method often suffers from numerical diffusion unless extremely fine mesh is used. If such extremely fine mesh is used, then Yang et al. (2020) demonstrated that the random-walk method can be

more efficient as it is free from numerical diffusion and the computation is restricted to regions where pollutant clouds exist. In practice, the mesh-based model has to adopt coarse meshes for the computational time to be affordable. Then, the dispersion and diffusion coefficients need to be specified by calibrating the computational results against measurements, and their values take into account the effect of numerical diffusion rather than truly reflect the physical processes. When taking such a strategy, the mesh-based model is often more efficient than the random-walk method.

This paper further develops the random walk model to simulate more complex hydro-environmental phenomena that involve the transport of non-conservative materials. In water quality modelling, there are three types of indicators of the water quality, including physical, chemical and biological indicators. Most of them represent non-conservative materials. For example, the concentration of Dissolved Oxygen (DO) is an essential indicator for analysing the nutrient cycle (Jha et al. 2007). The ability to maintain adequate DO is important for the waste assimilative capacity. Streeter and Phelps (1958) are the first to establish the relationship between the decay of organic waste, measured by the Biochemical Oxygen Demand (BOD), and the DO resource of the river. These chemical indicators quantify the amount of non-conservative substances in the water. However, most of the previous research on the random walk model only considers inert materials, without taking into account chemical and biochemical reactions. This paper first presents three ideal test cases to examine the capability of the random walk model for addressing the continuous release of non-conservative materials. Then, the model is applied to simulate the BOD-DO balance along a hypothetical river, with the analytical solutions as references. Finally, the developed scheme is used to predict the development of BOD and DO concentrations in the Thames Estuary, so as to examine the model's capability of handling the complex geometry with large tidal oscillations.

2. Depth-averaged random-walk model

2.1 Governing equations

The random walk model used in this paper is based on the depth-averaged advection-diffusion-reaction equation, which is a variant of the classical 2-D transport equation (Gresho & Sani 1998; Pu, et al. 2012). The pollutant substances are assumed to exactly follow the shallow flow in the advective stage, but the presence of the solute does not affect the water motion. Compared with turbulent diffusion and longitudinal dispersion, the molecular

diffusion can be neglected. Under these assumptions, the conservative formulation of the solute mass conservation can be cast as:

$$\frac{\partial S}{\partial t} + \frac{\partial (US)}{\partial x} + \frac{\partial (VS)}{\partial y} = \frac{\partial^2 (D_{xx} S)}{\partial x^2} + 2\frac{\partial^2 (D_{xy} S)}{\partial x \partial y} + \frac{\partial^2 (D_{yy} S)}{\partial y^2} + q_s \quad (1)$$

$$U = u + \frac{\partial D_{xx}}{\partial x} + \frac{\partial D_{xy}}{\partial y} + \frac{D_{xx}}{h}\frac{\partial h}{\partial x} + \frac{D_{xy}}{h}\frac{\partial h}{\partial y} \quad (2)$$

$$V = v + \frac{\partial D_{yy}}{\partial y} + \frac{\partial D_{xy}}{\partial x} + \frac{D_{yy}}{h}\frac{\partial h}{\partial y} + \frac{D_{xy}}{h}\frac{\partial h}{\partial x} \quad (3)$$

where $S = sh$, with h being the water depth and s being the depth-averaged concentration of the solute; t is time; u and v represent the flow velocities along x- and y-axis, respectively; q_s is the source term due to the pollutant release or biochemical reaction; U and V represent the modified advective velocities, which allow the particle-tracking scheme to use a random-walk technique designed for the solution of the classical transport process and for the simulation of diffusion (Hunter et al. 1993); D_{xx}, D_{xy}, D_{yx} and D_{yy} represent the dispersion-diffusion tensor of the depth-averaged mixing in Cartesian coordinates. The streamwise dispersion coefficient D_s and transverse diffusion coefficient D_t can be calculated as:

$$D_s = \varepsilon_s h u_*,\ D_t = \varepsilon_t h u_* \quad (4)$$

$$u_* = \frac{\sqrt{g}}{C} \cdot \sqrt{u^2 + v^2}, \quad C = \frac{h^{1/6}}{n} \quad (5)$$

where u_* is bed shear velocity; ε_s and ε_t are two non-dimensional coefficients quantifying the magnitude of streamwise dispersion and transverse diffusion, respectively. In Equation (5), C is the Chézy coefficient and n is the Manning roughness coefficient, both used to describe the bed friction in the flow. For straight open channel flows, ε_s and ε_t can be set to typical values of 13.0 and 1.2, respectively. For meandering natural free-surface flows, their values should be increased significantly. The relationship between the local streamwise-transverse coordinator and global Cartesian coordinates can be expressed as:

$$D_{xx} = D_s \cos^2\theta + D_t \sin^2\theta \quad (6)$$

$$D_{xy} = D_{yx} = (D_s - D_t)\sin\theta\cos\theta \quad (7)$$

$$D_{yy} = D_s \sin^2\theta + D_t \cos^2\theta \quad (8)$$

where $\theta = \arctan(v/u)$ is the angle between the flow direction and the x-axis.

According to the random walk method, *S*, which represents the amount of solute per unit horizontal area, can be approximated by a probability density function of the particles moving with some degree of randomness. In general applications, the water depth, modified advective velocities and dispersion-diffusion tensor should be obtained first by solving the depth-averaged Navier-Stokes equations, *i.e.* shallow water equations. Then, this depth-averaged random walk model is implemented by performing the advective, diffusive and reactive procedures successively in each time step, as explained in the following sections.

2.2 Advective process

Prior to the solution of the transport equation, the flow field should be solved first. For most shallow flow solvers, water depths and velocities are stored on discrete points in the computational domain. We assume that the water depth, flow velocity and dispersion-diffusion tensor are stored on Cartesian grid. To reconstruct a continuous variation of the flow field over the computational domain, we adopt bilinear interpolation in space. Taking the velocity at a point P*(x, y)* for example, the value is interpolated from the velocities at four nearby grid points $Q_{i,j}$, $Q_{i+1,j}$, $Q_{i,j+1}$, and $Q_{i+1,j+1}$, as illustrated in Figure 1.

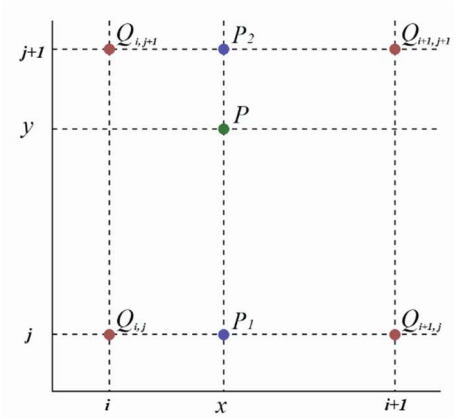

Figure 1. Bilinear interpolation

Three steps are involved in the spatial interpolation procedure. Firstly, we determine (U_{p1}, V_{p1}) on the southern side of the cell at a position aligned with $Q_{i,j}$ and $Q_{i+1,j}$ as follows:

$$U_{p1} = U_{i,j} + (U_{i+1,j} - U_{i,j})\left(\frac{x_p - x_{i,j}}{x_{i+1,j} - x_{i,j}}\right) \tag{9}$$

$$V_{p1} = V_{i,j} + (V_{i+1,j} - V_{i,j})\left(\frac{x_p - x_{i,j}}{x_{i+1,j} - x_{i,j}}\right) \tag{10}$$

Then, we determine (U_{p2}, V_{p2}) on the northern side of the cell at a position aligned with $Q_{i,j+1}$ and $Q_{i+1,j+1}$ as follows:

$$U_{p2} = U_{i,j+1} + (U_{i+1,j+1} - U_{i,j+1})(\frac{x_p - x_{i,j+1}}{x_{i+1,j+1} - x_{i,j+1}}) \quad (11)$$

$$V_{p2} = V_{i,j+1} + (V_{i+1,j+1} - V_{i,j+1})(\frac{x_p - x_{i,j+1}}{x_{i+1,j+1} - x_{i,j+1}}) \quad (12)$$

The third step involves the interpolation in the y-direction, giving (U_p, V_p) as:

$$U_p = U_{p1} + (U_{p2} - U_{p1})(\frac{y_p - x_{i,j}}{y_{i+1,j+1} - y_{i,j}}) \quad (13)$$

$$V_p = V_{p1} + (V_{p2} - V_{p1})(\frac{y_p - x_{i,j}}{y_{i+1,j+1} - y_{i,j}}) \quad (14)$$

The new particle position after the advective transport process can be expressed by Equation (15) using the second-order iterative technique.

$$x^a = x^{old} + \bar{U}\Delta t,\ y^a = y^{old} + \bar{V}\Delta t \quad (15)$$

where $\bar{U}$ and $\bar{V}$ are the two velocity components used in calculating a particle's advective displacement in each time step. To increase the order of accuracy, they are taken to be the time-averaged velocity within each time step.

$$\bar{U} = \frac{1}{2}\big(U(x^{old}, y^{old}, t) + U(x^a, y^a, t + \Delta t),\ \bar{V} = \frac{1}{2}\big(V(x^{old}, y^{old}, t) + V(x^a, y^a, t + \Delta t)\big) \quad (16)$$

2.3 Dispersion and diffusion process

Particles also undergo the dispersion and diffusion transport in each time step. The random streamwise and transverse velocities are calculated as follows.

$$U_s^d = r_s\sqrt{\frac{2D_s}{\Delta t}}\ ,\ V_t^d = r_t\sqrt{\frac{2D_t}{\Delta t}} \quad (17)$$

where the subscripts *s* and *t* represent the streamwise and transverse directions, respectively. The superscript *d* represents the diffusion-related velocity components. The random numbers r_s and r_t are independent of each other and follow a normal distribution with a mean of zero and a standard deviation of unity. According to the principles of tensor transformation between coordinate systems, the diffusion-dispersion process corresponds to the extra velocity components in the original Cartesian coordinate system:

$$U_x^d = U_s^d \cos\theta - V_t^d \sin\theta, V_y^d = U_s^d \sin\theta + V_t^d \cos\theta \quad (18)$$

Finally, the new position of the particle can be calculated as:

$$x^{new} = x^a + U_x^d \Delta t, y^{new} = y^a + V_y^d \Delta t \quad (19)$$

2.4 Reactive process

Most of the materials transported by the flow are not inert in the fluid, such as nitrogen, phosphorus, bacteria and dissolved oxygen. In order to predict the spatial and temporal development of these non-conservative substances, the sources term q_s is introduced in Equation (1). It represents the increase ($q_s > 0$) or decrease ($q_s < 0$) of the total amount of the solute because of chemical or biochemical reactions. For a substance subject to chemical or biological transformation, its decay or growth usually follows the principle of the first-order reaction:

$$q_s = -K_r S \quad (20)$$

where K_r is the decay rate or reaction constant. In the random walk model, an initial value of the mass $m_p^0 = \frac{M_0}{N}$ is assigned to every particle, where M_0 is the the total amount of solute material at time zero and N is the total number of particles. For the first-order decay processes, the mass of each particle is simply reduced by a fixed proportion at each timestep. For example, the mass of particle *P* at time *t* is expressed as:

$$m_p^{t-\tau+\Delta t} = m_p^{t-\tau} + \Delta t(-K_r m_p^{t-\tau}) \quad (21)$$

where τ in the superscript represents the time of the particle release so that the duration of this particle experiencing decay is (t - τ). For particles released at time zero, their value of τ is zero and they have experienced decay from time zero to the considered instant *t*. If particles are not released into the domain at the same time, such as in the situation of a continuous source, different particles carry different masses, and the concentration can be calculated via the probability density function weighted by the particles' masses.

2.5 Time advancement

When updating a particle's position and mass using the above method, only first order accuracy can be achieved. In the present implementation of the random walk model, a second-order Runge-Kutta time integration method is used. The time advancement from instant *t* to instant $t+\Delta t$ is carried out as follows:

$$x_p^{t+\Delta t} = x_p^t + \frac{1}{2}\Delta t(k_{11} + k_{12}) \quad (22)$$

$$y_p^{t+\Delta t} = y_p^t + \frac{1}{2}\Delta t(k_{21} + k_{22}) \quad (23)$$

$$m_p^{t+\Delta t} = m_p^t + \frac{1}{2}\Delta t(k_{31} + k_{32}) \quad (24)$$

$$k_{11} = \left(\frac{dx}{dt}\right)^t_{x_p,y_p},\ k_{21} = \left(\frac{dy}{dt}\right)^t_{x_p,y_p},\ k_{31} = \left(\frac{dm}{dt}\right)^t_{x_p,y_p} \quad (25)$$

$$k_{12} = \left(\frac{dx}{dt}\right)^{t+\Delta t}_{x_p+k_{11}\Delta t,y_p+k_{21}\Delta t},\ k_{22} = \left(\frac{dy}{dt}\right)^{t+\Delta t}_{x_p+k_{11}\Delta t,y_p+k_{21}\Delta t},\ k_{32} = \left(\frac{dm}{dt}\right)^{t+\Delta}_{x_p+k_{11}\Delta t,y_p+k_{21}\Delta t} \quad (26)$$

This is a second-order accurate iterative scheme, meaning that the total accumulated error is on the order of $O(\Delta t^2)$.

2.6 Treatment of moving boundaries

The wetting and drying phenomena is common in environmental flows, especially in shallow waters with uneven bottoms. A special treatment for this moving boundary is explained in detail in Liang et al. (2006). In the random walk model, a minimum water depth h_{min} is introduced, below which the bed is regarded to be day. The water depth at each particle's location is checked in each time step. If a particle is found to be on a dry bed, then the particle will be frozen to the position. The frozen particles are excluded in the advective and diffusive processes, but the reaction process is still considered on frozen particles. When the water depth is higher than h_{min}, the frozen particles are freed and then participate in the advective, diffusive and reactive processes.

3 Model refinement and verification

3.1 Continuous source

The present 2-D random walk model was first applied to the continuous release problem. A continuous discharge is released from the location (x_0, y_0) = (0, 400 m). The flow is uniform with u_0 = 1 m/s along the x-axis. The water depth is constant with h = 1 m and the Chézy coefficient is 40 $m^{1/2}/s$ over the whole test area. The constants for calculating the streamwise dispersion and transverse diffusion coefficients are set to be typical values of 13.0 and 1.2, respectively, for straight open channel flows. According to Equation (4-8), the mixing coefficients in this case are calculated to be $D_{xy} = D_{yx} = 0$, $D_{xx} = D_s = 1.020$ m^2/s, $D_{yy} = D_t =$ 0.094 m^2/s.

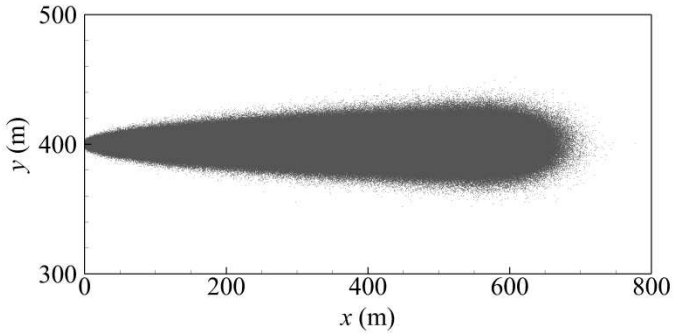

(a) Scatter of particles

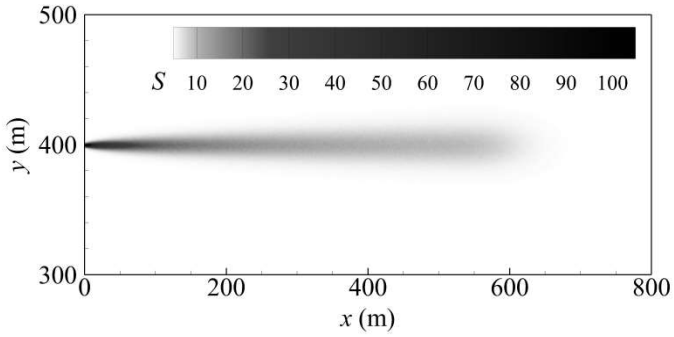

(b) Concentration distribution for the case of constant discharge rate

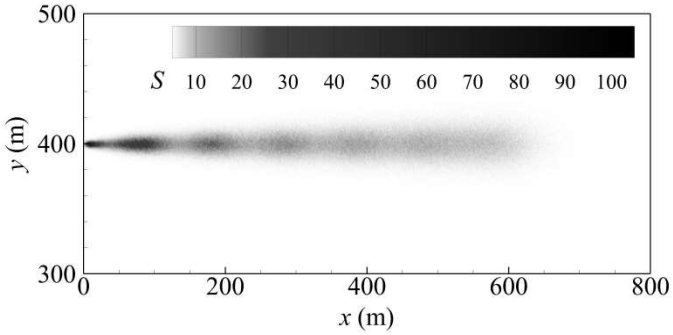

(c) Concentration distribution for the case of variant discharge rate

Figure 2 Continuous release problem in a uniform flow

Two pollutant discharge conditions are considered in this section. Firstly, the mass discharge rate $\dot{M}$ is constant at $\dot{M}_0 = 233.06$ kg/s. For this ideal case with uniform flow along the *x*-axis and constant mass discharge rate $\dot{M}$, the analytical solution can be expressed as:

$$S(x,y) = \frac{\dot{M}_0}{\sqrt{4\pi D_{yy} x u_0}} e^{-\frac{u_0 y^2}{4D_{yy}x}} \tag{27}$$

Secondly, the time-varying mass discharge rate is applied to the model. The mass discharge rate $\dot{M}$ is assumed to be a sinusoidal function of time, as seen in Equation (28).

$$\dot{M} = \dot{M}_0 \left(1 + \frac{1}{2}\sin\left(\frac{\pi t}{50}\right)\right) \tag{28}$$

The time step is $\Delta t = 1$ s. The number of particles released to the computational domain is 10^3 per time step. Whether the mass discharge rate is constant or time-varying, the scatter of particles is the same, as illustrated in Figure 2(a). The only difference is the mass associated to each particle. In the case of constant discharge rate, all the particles have the same mass. In the case of time-varying discharge rate, particles may carry different masses. The concentration contour 600 s after the start of the simulation is presented in Figures 2(b,c). It is notable that the concentration generally decreases away from the source and the centreline of the pollutant cloud is in the flow direction. The contour of the concentration for the time-varying mass discharge rate depicts a certain degree of periodic oscillation along the flow.

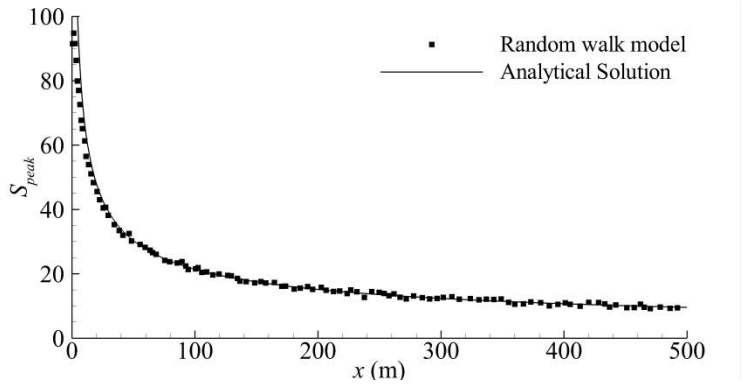

(a) Constant mass discharge

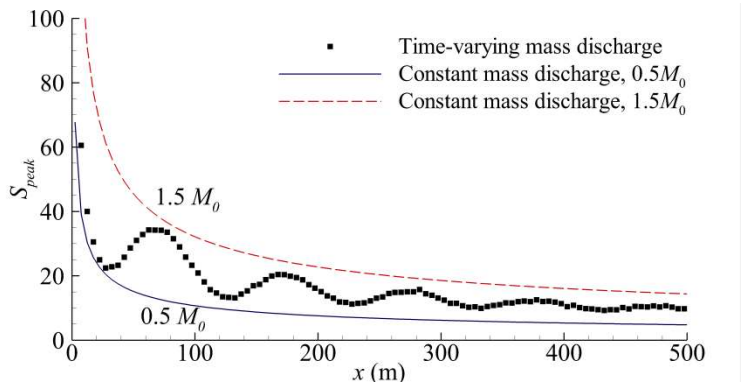

(b) Time-varying mass discharge

Figure 3 Profiles of concentrations along the x-axis at y = 400 m.

Figure 3(a) shows the concentration along centreline of the pollutant could predicted by the random walk model, which is perfectly consistent with the analytical solution. When the discharge rate is not constant, then there is no analytical solution, The black square symbols in Figure 3(b) represent the variation of concentrations along the centreline of the pollutant cloud predicted by the random walk model with time-varying mass discharge rate. Here, the time-averaged flow rate is the same as that in Figure 3(a), but it varies from $0.5\dot{M}$ and $1.5\dot{M}$.

The predicted results show an overall trend of decrease along the flow but are accompanied by periodic fluctuations. The predicted concentrations are bounded by the analytical solutions with constant mass discharge rates of $0.5\dot{M}$ and $1.5\dot{M}$, which are also plotted in Figure 3(b) as solid and dashed lines, respectively.

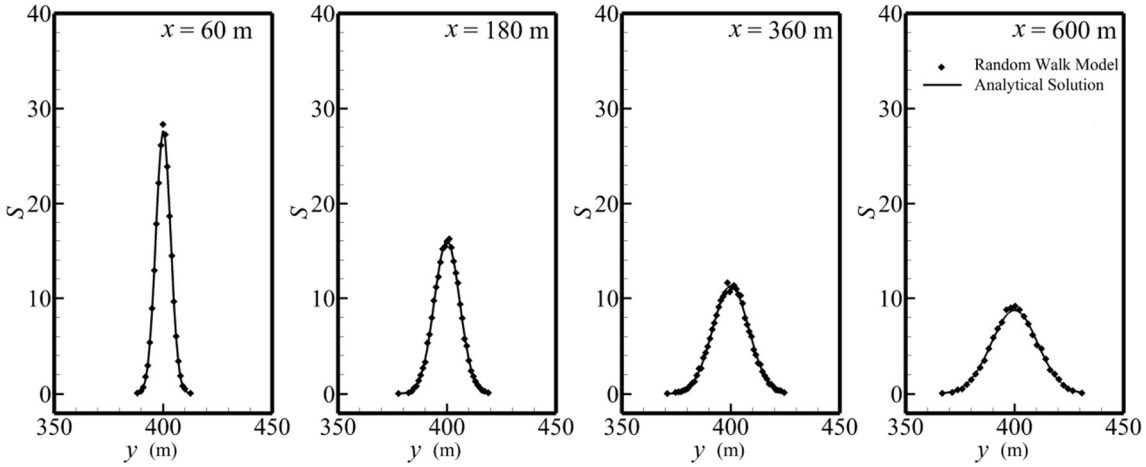

Figure 4 Cross-flow concentration distribution at four downstream sections at t = 600 s

As analytical solutions exist for case 1, quantitative comparisons are made between the predicted and theoretical concentration distributions in the cross-flow directions. Figure 4 illustrates the concentration profiles at four sections downstream of the source. The concentration distribution follows a Gaussian distribution in the cross-flow direction. The peak concentration gradually decreases while the distribution range increases with the location moving farther away from the discharge point. These results predicted by the random walk model, indicated by square symbols, agree well with the analytical solution, indicated by solid lines.

3.2 Mass decay

Another ideal test case with known analytical solutions is used in this section to verify the random walk prediction quantitatively. The flow is uniform with u_0 = 1 m/s along the x-axis. The water depth h = 1 m, and the Chézy coefficient is 40 $m^{1/2}$/s over the whole test area. The values of ε_s and ε_t are set to be 13.0 and 1.2, respectively. Then, the mixing coefficients are calculated to be $D_{xy} = D_{yx} = 0$, $D_{xx} = D_s = 1.020$ m²/s, $D_{yy} = D_t = 0.094$ m²/s. In this case, the total amount of solute material of M = 233.06 kg is released suddenly at the origin. The material is assumed to be subject to biological decay, which can be expressed as the first-order reaction function, *i.e.* Chick's Law, as given in Equation (20). Then, the analytical solution to this 2-D reaction case can be written as:

$$S(x,y,t) = \frac{M/h}{4\pi t\sqrt{D_{xx}D_{yy}}} e^{-\frac{(x-x_0-ut)^2}{4D_{xx}t} - \frac{(y-y_0)^2}{4D_{yy}t} - K_r t} \quad (29)$$

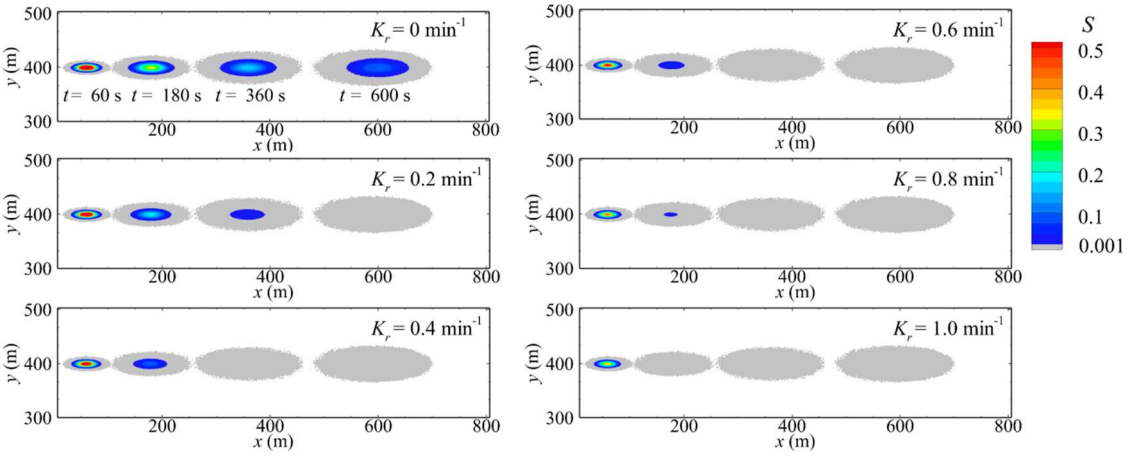

Figure 5 Evolution of the pollutant cloud at 30 s, 180 s, 360 s and 600 s

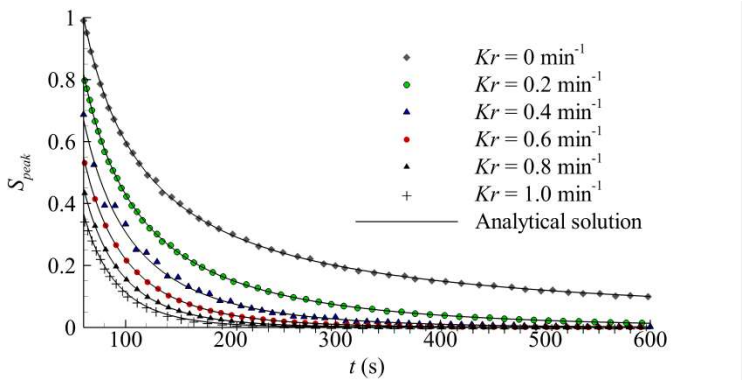

Figure 6 Time variations of the peak concentration of the pollutant cloud

The time step Δt of 1 s is adopted. The number of particles released to the computational domain is 2.33×10^6. As all the particles are released at $t = 0$, the value of τ in Equation (21) is zero. Each plot in Figure 5 corresponds to one decay rate, which includes the predicted concentration contours at four instants: t = 60 s, t = 180 s, t = 360 s and t = 600. A total of six decay rates are considered, *i.e.* K_r = 0 min^{-1}, 0.2 min^{-1}, 0.4 min^{-1}, 0.6 min^{-1}, 0.8 min^{-1} and 1.0 min^{-1}, hence the six plots. In general, these concentration contours are elliptical. Due to the much smaller level of transverse diffusion than that of streamwise dispersion, the solute clouds experienced rapid elongation along the flow direction. The grey colour is used to represent the non-zero solute concentration that is lower than 0.001 units, indicating where the pollutant is nearly assimilated into the ambient water. In theory, the concentration should be non-zero everywhere in the domain. However, there is a minimum concentration that can be numerically resolved by the random walk method, which is determined by the number of

particles deployed. No particles can reach the regions with concentrations smaller than the minimum value, and thus the concentration in these regions will be deemed to be zero in the random walk simulation. A qualitative comparison of the predictions with different decay rates highlights the effect of mass decay over time, which becomes more and more apparent as time progresses. The high-concentration area shrinks rapidly with time, especially with a high decay rate of the non-conservative solute. Taking $K_r = 0.2$ min^{-1} for example, the concentration everywhere in the domain falls below 0.001 units at t = 600 s. As the decay coefficient increases to $K_r = 1.0$ min^{-1}, it takes only 180 s for the concentration everywhere in the domain to fall below 0.001. The quantitative analysis is illustrated in Figure 6, which compares the theoretical and predicted maximum concentrations. The results generated by the random walk model, indicated by symbols, are in perfect agreement with analytical solutions, indicated by solid lines. When the solute is assumed to be conservative ($K_r = 0$), the combination of computational parameters produces a peak concentration of unity at t = 60 s. This peak concentration decreases more rapidly with the increase of the decay rate.

3.3 BOD-DO model

In this section, the random walk model is applied to predict the variations of the BOD and DO concentrations in uniform flows. An aerial view of a narrow river is illustrated in Figure 7, together with the key parameters. In this case, the flow is uniform with u_0 = 0.25 m/s along the river. We use the x to designate the streamwise coordinate in this one-dimensional river model, so x-axis may be curved rather than straight. The water depth is constant at h = 1 m. The traditional BOD-DO interaction model was established by Streeter and Phelps (1958). The concentration of the DO may increase due to re-oxygenation and photosynthesis at the free surface. The wastewater is assumed to be continuously discharged into the narrow river at a constant rate. The distribution of the solute is steady and can be assumed to be totally mixed over a cross-section. Then, the relationship between the BOD and DO concentrations can be simplified as follows:

$$U\frac{dS_{BOD}}{dx} = -K_r S \tag{30}$$

$$U\frac{dS_{DO}}{dx} = K_a(S_{DOsat} - S_{DO}) - K_r S_{BOD} \tag{31}$$

The analytical solution to the Equations (30-31) can be expressed as:

$$S_{BOD} = S_{BOD0}e^{-K_r x/U} \tag{32}$$

$$S_{DO} = S_{DOsat} - S_{BOD}\ \frac{K_r}{K_a - K_r}\left[e^{-\frac{K_r x}{U}} - e^{-\frac{K_a x}{U}}\right] - (S_{DOsat} - S_{DO0})e^{-K_a x/U} \tag{33}$$

where S_{DO0} and S_{BOD0} are DO and BOD concentrations, respectively, at origin $x = 0$; S_{DOsat} is the saturated DO concentration in water; K_r is the BOD deoxygenation rate and K_a is the re-oxygenation rate.

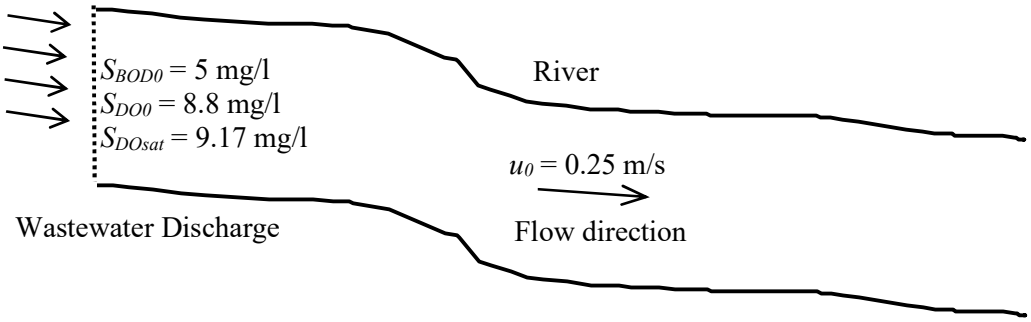

Figure 7 Continuous discharge of wastewater in the uniform flow

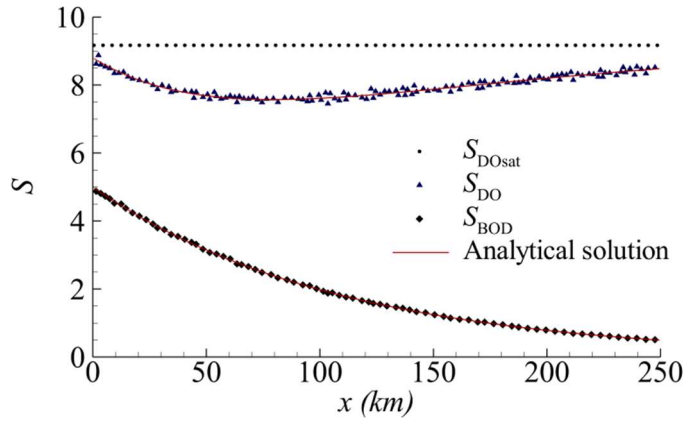

(a) Profile of BOD and DO concentrations

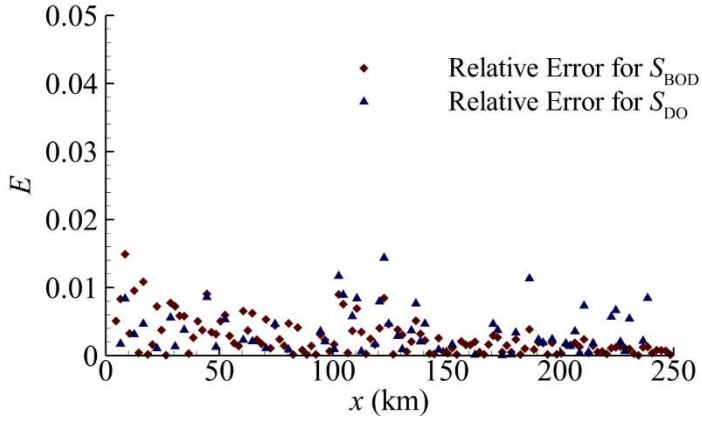

(b) Relative errors for BOD and DO predictions

Figure 8 Variations of BOD and DO concentrations and prediction errors along *x*-axis

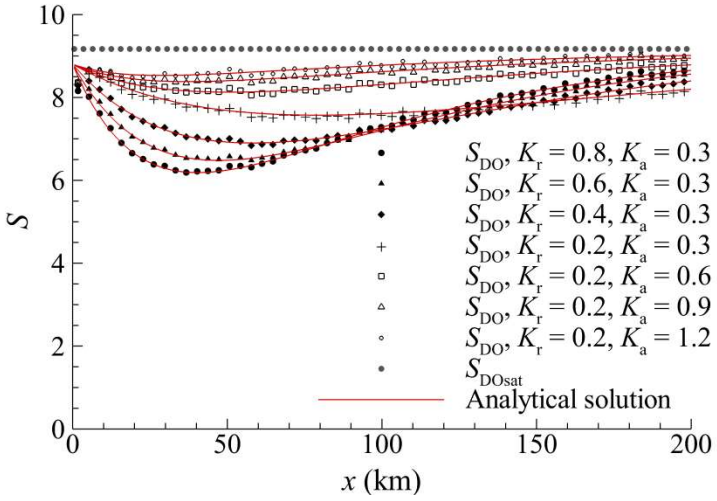

(a) Profiles of DO concentration

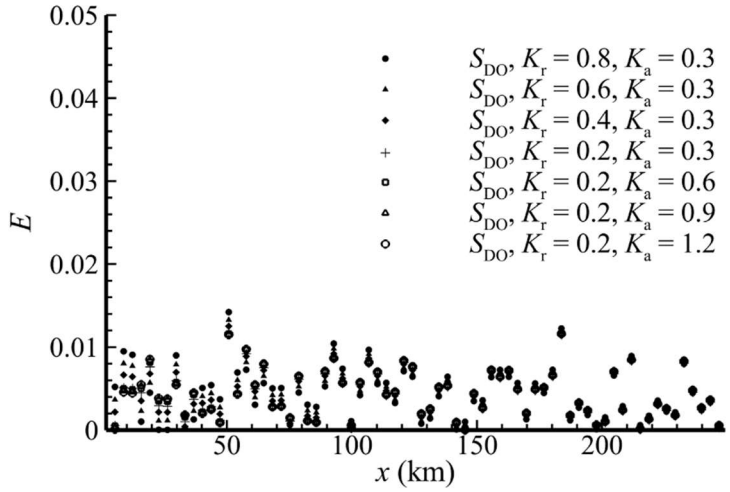

(b) Relative errors for DO predictions

Figure 9 Variations of DO concentration and prediction errors along *x*-axis for different combinations of K_r and K_a.

In random walk modelling, the original unsteady advection-diffusion-reaction equations are solved. Two sets of particles are used as BOD and DO indicators respectively. The mass of a particle at time *t* is updated using Equations (34-35), which are the discrete form of the reaction terms on the right-hand sides of Equations (30-31).

$$m_{BOD}(t + \Delta t) = m_{BOD}(t) + \Delta t(-K_r m_{BOD}(t)) \tag{34}$$

$$m_{DO}(t + \Delta t) = m_{DO}(t) + \Delta t(K_a m_{DOsat} - K_a m_{DO}(t) - K_r m_{BOD}(t + \Delta t)) \tag{35}$$

In the simulation, K_r is set to be 0.2 per day while K_a is set to be 0.3 per day. The sewage effluent contains BOD of 5 mg/l and DO of 8.8 mg/l. The saturation concentration of oxygen in water at 20 ºC is 9.17 mg/l. The time step is $\Delta t = 1$ s. The number of particles released to the computational domain is 10^3 per time step. Figure 8(a) compares the numerical results of the random walk model, indicated by symbols, and the analytical solutions, indicated by solid lines, for the corresponding BOD decay curve and DO sag curve. It can be seen that the predicted results agree well with the analytical solutions. An error analysis is performed by calculating the relative error of each predicted concentration as follows.

$$E = \frac{|S_{predicted} - S_{analytic}|}{S_{analytical}} \tag{36}$$

where E gives the relative difference between the predicted concentration $S_{predicted}$ and the analytical solution $S_{analytical}$. As seen in Figure 8(b), the relative error of any predicted concentration, in comparison with the analytical value, is less than 1.6% in all cases.

Figure 9(a) illustrates the DO concentration profile with a series combination of BOD deoxygenation rate K_r and re-oxygenation rate K_a. As K_a increases, the DO distribution curve becomes flatter and approaches the value of S_{DOsat} more rapidly. On the contrary, the DO curve sags more and approaches the asymptotic value more slowly when the BOD deoxygenation rate K_r gets larger. It can be concluded that the BOD deoxygenation rate K_r has a greater influence on the DO concentration. Figure 9(b) presents the error analysis for the different combinations of the reaction constants. Again, all the relative errors are less than 1.6%. Overall, the numerical results predicted by the current random walk model agree well with the theoretical solutions.

4. Model application to Thames Estuary

In the previous section, the performance of the random walk model has been tested in three idealised examples. In this section, the validated random walk model is applied to predict the BOD-DO interaction in the Thames Estuary. The Thames Estuary is located in the southeast of the UK, where the River Thames meets the North Sea. The unsteady flow field has been obtained by solving the shallow water equations using the TVD-MacCormack scheme (Mingham et al. 2001, Liang et al. 2006 and 2010b) on rectangular mesh. This algorithm is a modification of the widely-used MacCormack scheme by adding an extra step according to the total variation diminishing (TVD) principle. This method has been widely used for simulating hydro-environmental dynamics and is taken as a representative mesh-based method here. Figure 10 presents a typical water depth distribution in the Thames Estuary. In

terms of the fluvial inputs from upstream, only the River Thames and River Medway are considered in the simulation. A number of assumptions are adopted in this real-world example. The variations of the water level at the seaward boundaries are assumed to follow a sinusoidal function. The average sea level is assumed to be 0.05 m above the Newlyn Datum, and the tidal period is 12 h with amplitude of 3.02 m. Manning roughness values are specified according to the bed condition. The value for the normal seabed is 0.02 s/m$^{1/3}$, while the value for tidal floodplains covered with vegetation is 0.13 s/m$^{1/3}$. The computational mesh used by the shallow water solver consists of 1250 ×500 square elements of equal size with a side length of 80 m. The detailed computational conditions and the verification of the computed flow field can be found in Liang et al. (2010a, 2010b). The time variations of the velocities and water depths stored on this mesh are fed into the random walk model to drive the pollutant transport processes. The time step is set to be 1 s in the random walk model. Typical values of 13.0 and 1.2 are used again for the longitudinal dispersion and turbulent diffusion coefficients, respectively.

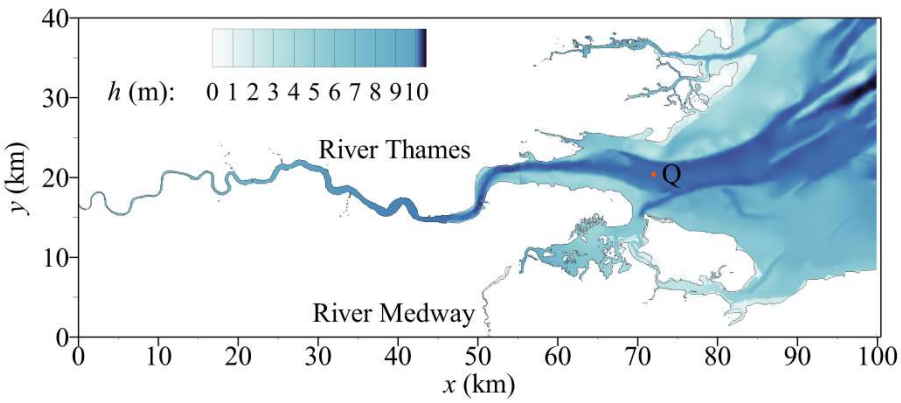

Figure 10 Typical water depth distribution in the Thames Estuary, superimposed with the discharge point Q

Two hypothetical release scenarios are considered. The first scenario is consistent with previous research in Liang et al. (2010b) for comparison purpose. It is assumed that the waste effluent is suddenly discharged into the tidal flow from location Q (x_0, y_0) = (72 km, 20.4 km) within 10 min. The total number of particles released is 1.95×10^5. Only one non-conservative material is considered in this scenario. The variation of the total discharge rate Q_s with time is shown in Figure 11. In the mesh-based modelling, the discharge is introduced to a computational element and so it is equal to q_s times the area of the element. In the random walk method, no mesh is used, and the effluent is exactly located at point (x_0, y_0).

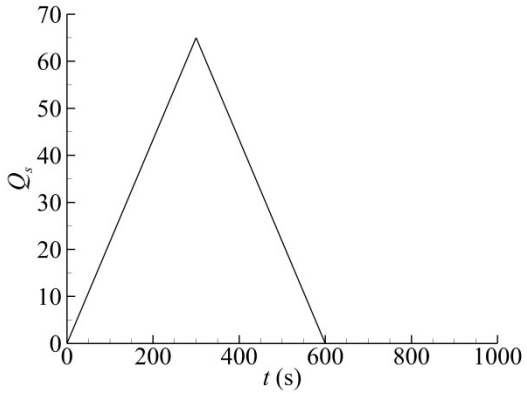

Figure 11 Total discharge rate Q_s at release point Q (x_0, y_0) = (72 km, 20.4 km)

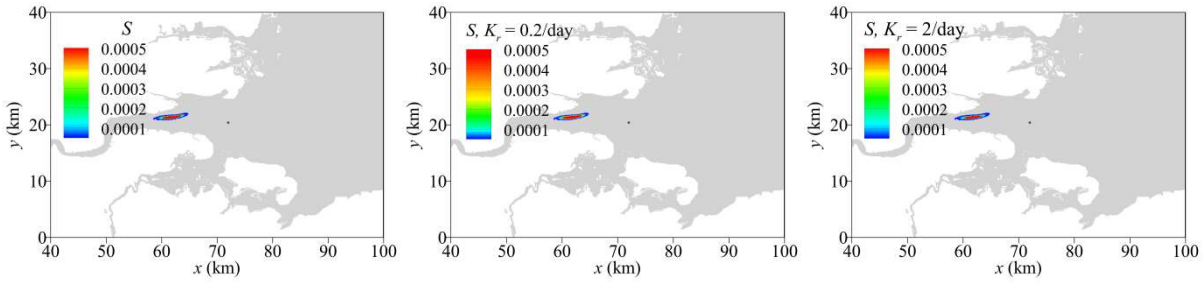

(a) $K_r = 0$ (b) $K_r = 0.2$/day (c) $K_r = 2$/day

Figure 12 Snapshots of solute clouds in the Thames Estuary 3 hours after the release

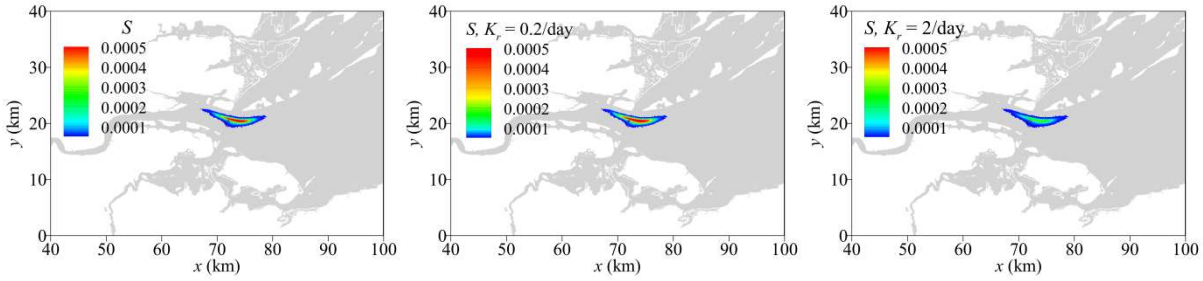

(a) $K_r = 0$ (b) $K_r = 0.2$/day (c) $K_r = 2$/day

Figure 13 Snapshots of solute clouds in the Thames Estuary 9 hours after the release

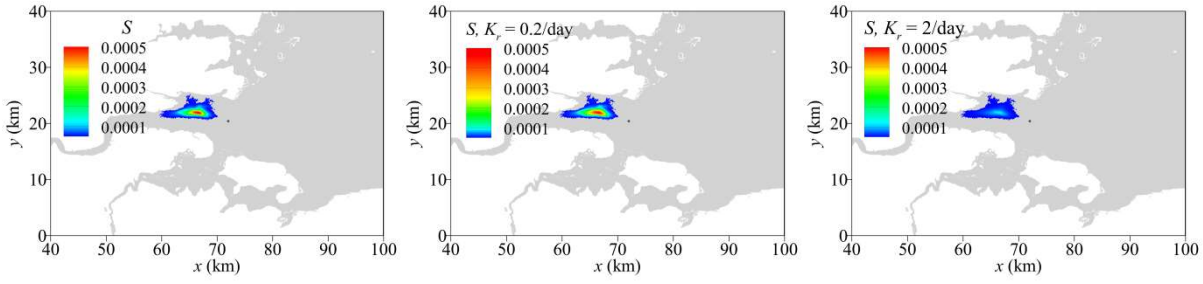

(a) $K_r = 0$ (b) $K_r = 0.2$/day (c) $K_r = 2$/day

Figure 14 Snapshots of solute clouds in the Thames Estuary 18 hours after the release

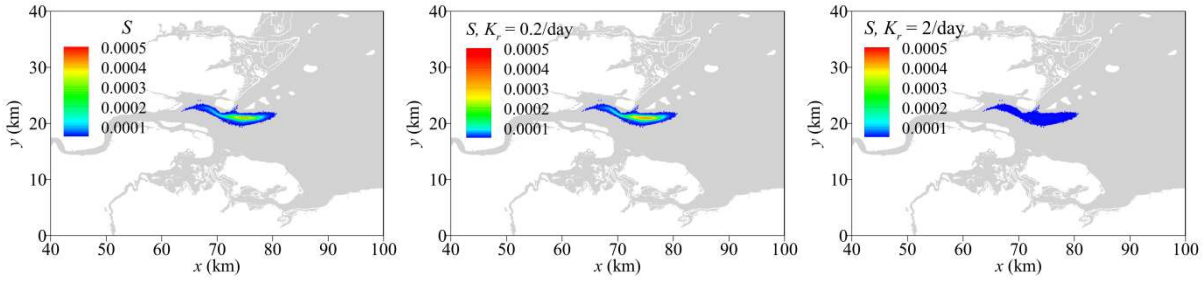

(a) $K_r = 0$ (b) $K_r = 0.2$/day (c) $K_r = 2$/day

Figure 15 Snapshots of solute clouds in the Thames Estuary 24 hours after the release

Figures 12-15 display a sequence of the concentration snapshots over the domain predicted by the 2-D random walk model. The grey colour represents the wet areas where the domain is occupied with water. The ebbing stage can be seen in Figures 12 and 14, while the flooding stage can be seen in Figures 13 and 15. As expected, the pollutant cloud oscillates back and forth with the tidal currents. In the first tidal cycle, the solute spreads over a broader area and becomes less concentrated as time progresses. The mesh-based TVD-MacCormack method had been applied to the same case in Liang et al. (2010b). By comparison, the random walk model gives an even higher resolution of the concentration distribution, as the random walk method suffers no numerical diffusion. On the contrary, the mesh-based approaches suffer from numerical diffusion unless the computational mesh is very fine. As for the computational cost, it depends on the number of particles and the time step used in the random walk modelling. The current simulation time is around 8 hours on a Dell Optiplex 790 computer for 48 hours of the transport process. The substance released in the tidal flow is assumed to be subject to biological transformation. The decay is expressed as the first-order reaction function, as shown in Equation (20). In Figures 12-15, each graph shows the predicted concentration contours with one decay rate at one instant. It can be seen that the concentration of non-conservative solute decreases rapidly with the increase of the decay rate and with the increase of time. The good comparison between predictions using this model and those based Euler methods indicates that the current random walk model is capable of modelling the transport of non-conservative materials in real-world scenarios with unsteady flows over uneven bed elevations and irregular geometries.

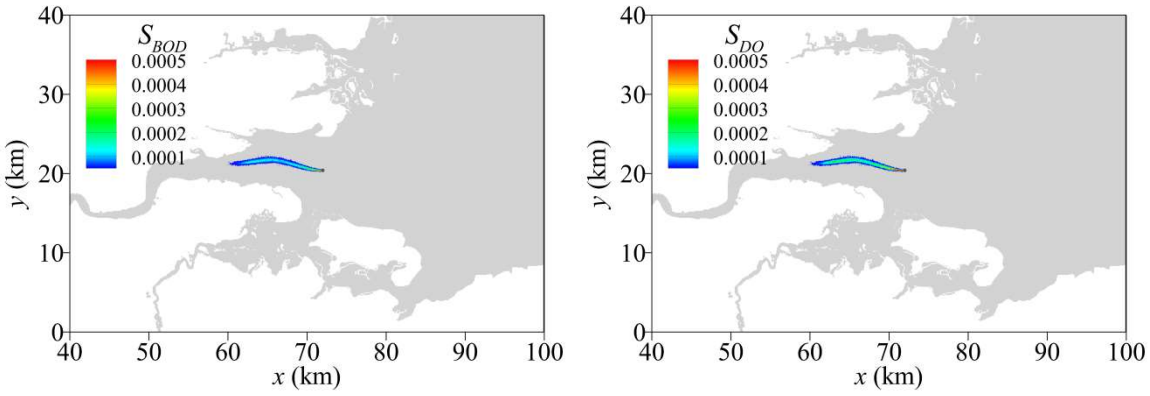

(a) t = 3 hours

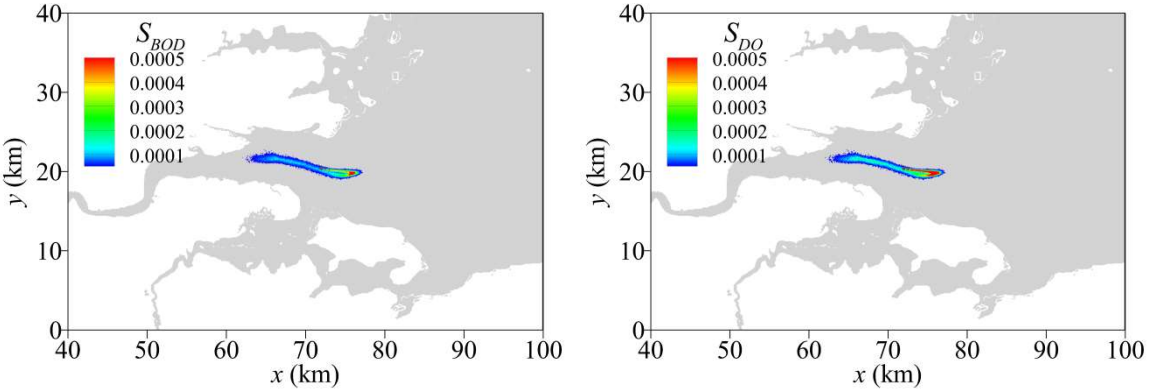

(b) t = 6 hours

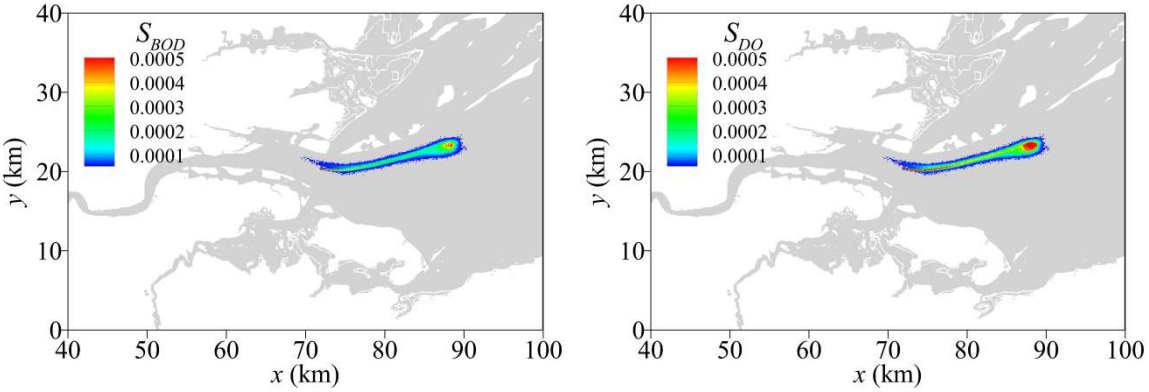

(c) t = 9 hours

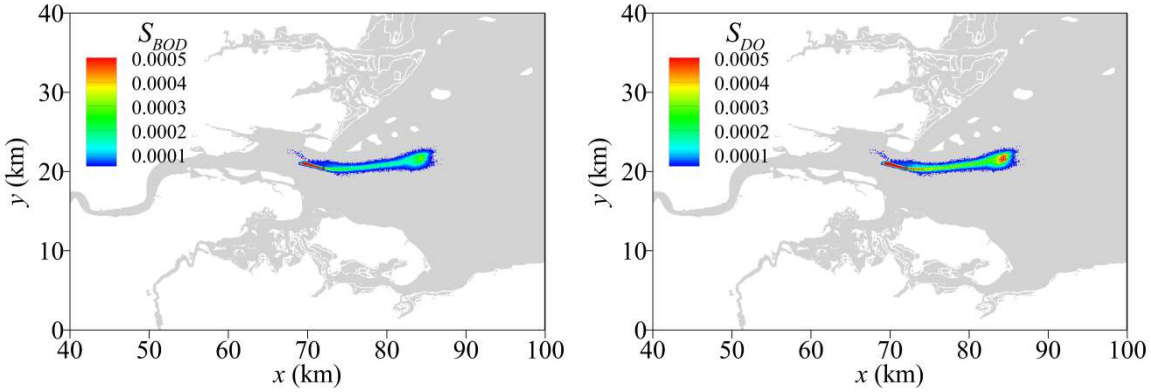

(d) t = 12 hours

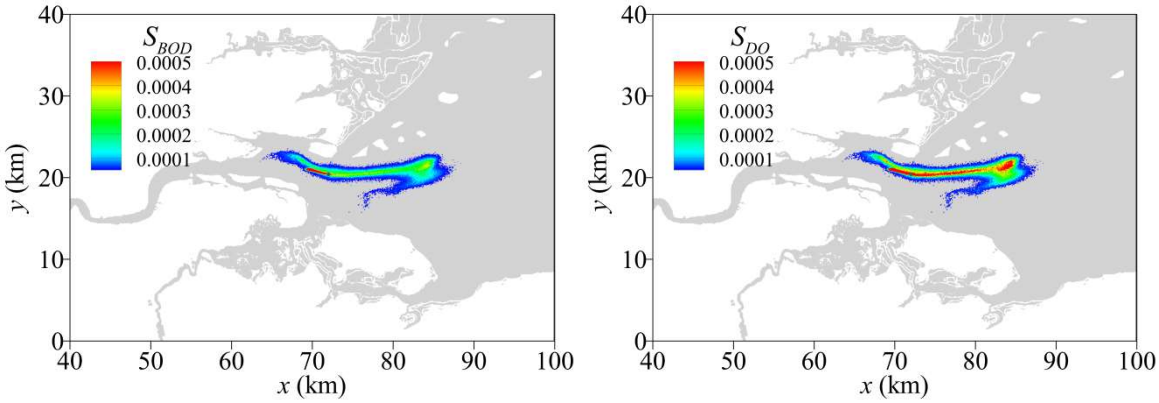

(e) t = 24 hours

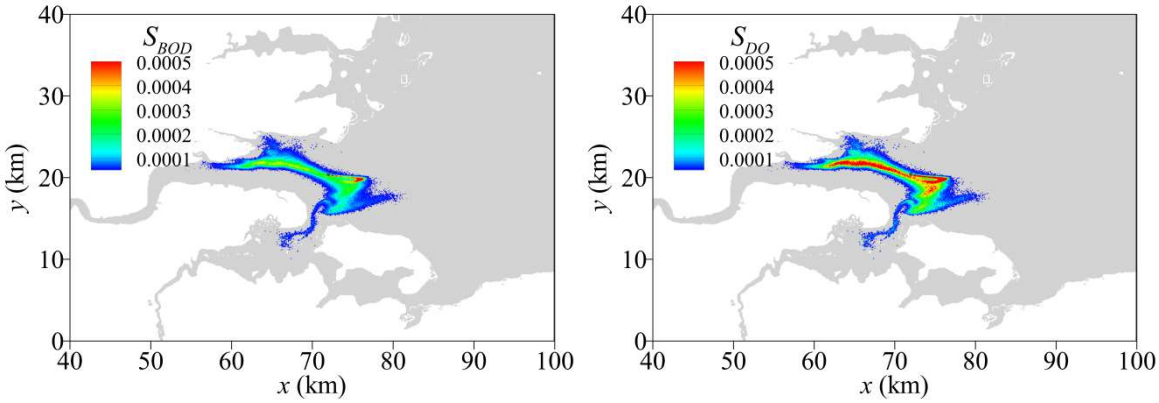

(f) t = 30 hours

Figure 16 Snapshots of the BOD (left) and DO (right) distributions in the Thames Estuary

The other release scenario considered is that the wastewater is continuously discharged into the Thames estuary. Both the BOD and DO concentrations are considered to examine the 2-D random walk model under this complicated tidal flow condition. In the simulation, K_r is set to be 0.2 per day while K_a is set to be 0.3 per day. The wastewater contains BOD of 5

mg/l and DO of 8.8 mg/l at the release point. The saturation concentration of oxygen in water at 20 °C is 9.17 mg/l. The number of particles released per time step is set to be 10^3. Figure 16 shows the snapshots of BOD and DO concentration fields at six instants. At t = 3 hours, the solute cloud spreads from the release point to the upper reaches of the River Thames. It is notable that the closer to the release point, the higher the concentration. The results at this instant are similar to the trend observed in Figure 2(b). After a half tidal cycle, as seen in Figure 16 (b), the clouds make a sharp U-turn and move towards the North Sea. Such a behaviour is reasonable as flow field changes direction as the tide switches into the ebbing stage. As seen in Figure 16 (c) and (d), there are two locally high-concentration patches in the DO concentration contours at 9 and 12 hours, one at the release point and the other at the location (x, y) = (88 km, 23 km) where the pollutant returns from the North Sea during the second half of the tidal cycle. At t = 30 hours, Figure 16(f) shows that the wastewater reaches the mouth of the River Medway. The solute cloud continues to oscillate back and forth with the tidal currents and spreads over a broader area as time progresses.

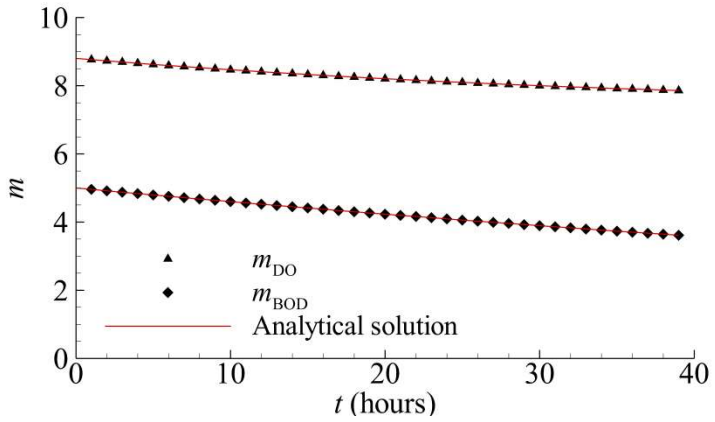

Figure 17 Mass variations of the BOD and DO attached to each particle

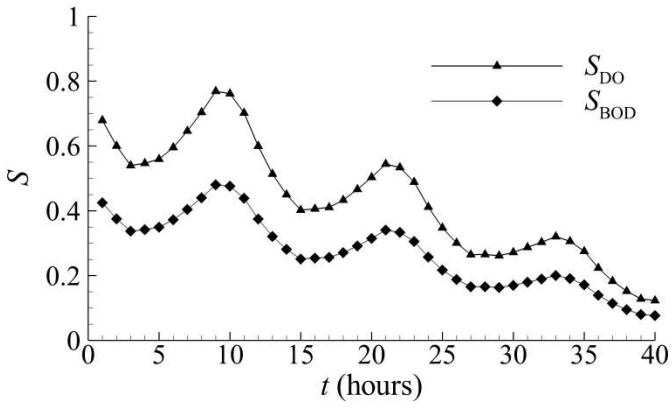

Figure 18 Time developments of the BOD and DO peak concentration in the Thames Estuary

Figure 17 compares the BOD and DO mass variations predicted by the random walk model with the analytical solutions. The numerical results, indicated by symbols, are in good agreement with analytical solutions, indicated by solid lines. In the previous discussion, the solute clouds oscillate back and forth with the tidal currents and become less concentrated as time progresses. Such phenomena are correspondingly evident in Figure 18. The temporal evolution of the maximum concentration is subject to periodic fluctuations, although an overall downward trend is evident. The period of 12 hours is consistent with the period of the tide flow.

5. Conclusions

The depth-averaged random walk model is developed to investigate unsteady solute transport processes in shallow water flows. Idealised cases are modelled to examine the capability of the present random walk method in addressing the instantaneous and continuous release of non-conservative substances in the simulations. The model was first applied to an ideal continuous release problem. The influence of the decay rate on the predictions is also investigated in the second test case. Then, the model is applied to solve a hypothetical BOD-DO balance problem in a one-dimensional uniform flow. The numerical predictions of the solute advection/diffusion/reaction processes are in good agreement with analytical solutions. Finally, the validated random walk model is successfully applied to predict two scenarios in the Thames Estuary, including the short-duration and continuous release cases. For the case of short-duration release of a conservative material, the random-walk predictions agree well with the conventional numerical results based on fine meshes. In the case of continuous discharge of wastewater into the Thames Estuary, the coupling of the BOD and DO is satisfactorily reproduced. The peak concentration of the degradable solute periodically fluctuates with time, with a period consistent with the specified tidal period.

The model developed in this paper is shown to be capable of modelling continuous release of non-conservative pollutants and the interaction between pollutants. To the best knowledge of the authors, it is the first time that the random-walk method is applied to such situations. In this feasibility study of the newly developed random walk algorithm, only a maximum of two non-conservative pollutants are considered. In the future, we will extend the present random-walk model to include more water quality indicators capable of conducting water quality analyses in more complicated real-world situations.

Acknowledgments

The work has been supported by the Royal Academy of Engineering UK-China Urban Flooding Research Impact Programme (No. UUFRIP\100051), the Ministry of Education and State Administration of Foreign Experts Affairs 111 Project (No. B17015), the Cambridge Tier-2 system operated by the University of Cambridge Research Computing Service (http://www.hpc.cam.ac.uk) funded by EPSRC Tier-2 capital grant EP/P020259/1 and the China Scholarship Council (No. 201708060090)

References

Benkhaldoun, Fayssal, Elmahi Imad, and Seaı Mohammed. "Well-balanced finite volume schemes for pollutant transport by shallow water equations on unstructured meshes." Journal of computational physics 226.1 (2007): 180-203.

Burguete, J., García Navarro P., and Murillo J.. "Numerical boundary conditions for globally mass conservative methods to solve the shallow water equations and applied to river flow." International journal for numerical methods in fluids 51, no. 6 (2006): 585-615.

Gresho P M, Sani R L. Incompressible flow and the finite element method. Volume 1: Advection-diffusion and isothermal laminar flow[J]. 1998.

Gupta, Indrani, Dhage Shivani, Chandorkar A. A., and Srivastav Anjali. "Numerical modeling for Thane creek." Environmental Modelling & Software 19, no. 6 (2004): 571-579.

Hunter, J. R. , Craig, P. D. , & Phillips, H. E. On the use of random walk models with spatially variable diffusivity. Journal of Computational Physics, 106, no. 2 (1993): 366-376.

Israelsson, Peter H., Kim Young Do, and Adams E. Eric. "A comparison of three Lagrangian approaches for extending near field mixing calculations." Environmental Modelling & Software 21.12 (2006): 1631-1649.

Jha, Ramakar, Ojha C. S., and Bhatia K. K.. "Development of refined BOD and DO models for highly polluted Kali River in India." Journal of Environmental Engineering 133, no. 8 (2007): 839-852.

Kazemi, Ehsan, Nichols Andrew, Tait Simon, and Shao Songdong. "SPH modelling of depth‐limited turbulent open channel flows over rough boundaries." International journal for numerical methods in fluids 83, no. 1 (2017): 3-27.

Liang, D., Falconer, R. A. & Lin, B. Comparison between TVD-MacCormack and ADI-type solvers of the shallow water equations. Advances in Water Resources, 29, no. 12(2006): 1833–1845.

Liang D, Carroll W and McRobie A. Some considerations of tidal flood risk in Thames estuary. Proceedings of the 9th international conference on hydroinformatics, Tianjin, China, 2010a, pp1959-1967.

Liang, D., Wang, X., Falconer, R. A. & Bockelmann-Evans, B. N. Solving the depth-integrated solute transport equation with a TVD-MacCormack scheme. Environmental Modelling & Software, 25, no, 12(2010b): 1619–1629.

Liang, D., Wu, X. “A random walk simulation of scalar mixing in flows through submerged vegetations.” Journal of hydrodynamics, 26(3) (2014): 343-350.

Lin, B. & Falconer, R. A. Tidal flow and transport modeling using ULTIMATE QUICKEST scheme. Journal of Hydraulic Engineering, 123, no. 4 (1997): 303–314.

Mingham, C. G., Causon, D. M. & Ingram, D. M. A TVD MacCormack scheme for transcritical flow. Proceedings of the Institution of Civil Engineers-Water and Maritime Engineering, 148, no. 3 (2001), 167–175.

Murillo, J., García Navarro, P., Burguete, J., & Brufau, P. (2006). A conservative 2D model of inundation flow with solute transport over dry bed. International Journal for Numerical Methods in Fluids, 52, no. 10 (2006), 1059-1092.

Murillo, J., Burguete J., Brufau P., and García Navarro Pilar. "Coupling between shallow water and solute flow equations: analysis and management of source terms in 2D." International journal for numerical methods in fluids 49, no. 3 (2005): 267-299.

Phelps, Earle B., and Streeter, H. W. A study of the pollution and natural purification of the Ohio River. US Department of Health, Education, & Welfare, 1958.

Pu, Jaan Hui, Cheng, Nian-Sheng, Tan, Soon Keat, and Shao, Songdong. "Source term treatment of SWEs using surface gradient upwind method." Journal of hydraulic research 50, no. 2 (2012): 145-153.

Pu, Jaan Hui. "Conceptual hydrodynamic-thermal mapping modelling for coral reefs at south Singapore sea." Applied Ocean Research 55 (2016): 59-65.

Pu, Jaan H., Huang, Yuefei, Shao, Songdong, and Hussain, Khalid. "Three-Gorges Dam fine sediment pollutant transport: turbulence SPH model simulation of multi-fluid flows." Journal of Applied Fluid Mechanics, 9, no. 1 (2016): 1-10.

Wu, Xuefei, Liang, Dongfang, and Zhang, Geliang. "Estimating the accuracy of the random walk simulation of mass transport processes." Water research 162 (2019): 339-346.

Yang, F., Liang, D. & Xiao, Y. Influence of Boussinesq coefficient on depth-averaged modelling of rapid flows. Journal of Hydrology, 559 (2018):909–919.

Yang, F., Liang, D., Wu, X., & Xiao, Y. On the application of the depth-averaged random walk method to solute transport simulations. Journal of Hydroinformatics, 22, no .1 (2020): 33-45.

Yuan, Dekui. Development of an integrated hydro-environmental model and its application to a macro-tidal estuary. PhD thesis, Cardiff University, 2007

Zheng, X., Shao, S., Khayyer, A., Duan, W., Ma, Q., and Liao, K. "Corrected first-order derivative ISPH in water wave simulations." Coastal Engineering Journal 59, no. 01 (2017): 1750010.